

NASA/TM-1999-209838



Active Control of Flow Separation Over an Airfoil

*S. S. Ravindran
Langley Research Center, Hampton, Virginia*

National Aeronautics and
Space Administration

Langley Research Center
Hampton, Virginia 23681-2199

December 1999

Available from:

NASA Center for AeroSpace Information (CASI)
7121 Standard Drive
Hanover, MD 21076-1320
(301) 621-0390

National Technical Information Service (NTIS)
5285 Port Royal Road
Springfield, VA 22161-2171
(703) 605-6000

Active Control of Flow Separation Over An Airfoil

S. S. Ravindran*[†]
 NASA Langley Research Center
 Hampton, Virginia

Abstract

Designing an aircraft without conventional control surfaces is of interest to aerospace community. In this direction, smart actuator devices such as synthetic jets have been proposed to provide aircraft maneuverability instead of control surfaces. In this article, a numerical study is performed to investigate the effects of unsteady suction and blowing on airfoils. The unsteady suction and blowing is introduced at the leading edge of the airfoil in the form of tangential jet. Numerical solutions are obtained using Reynolds-averaged viscous compressible Navier-Stokes equations. Unsteady suction and blowing is investigated as a means of separation control to obtain lift on airfoils. The effect of blowing coefficients on lift and drag is investigated. The numerical simulations are compared with experiments from the Tel-Aviv University (TAU). These results indicate that unsteady suction and blowing can be used as a means of separation control to generate lift on airfoils.

Nomenclature

A, B flux Jacobian
 C_L lift coefficient
 C_μ unsteady momentum blowing coefficient,
 $2(H/c) (U_{\text{jet}}/U_\infty)^2$
 $\langle C_\mu \rangle$ steady momentum blowing coefficient,
 $2(H/c) (\langle u'_{\text{jet}} \rangle / U_\infty)^2$

C_D drag coefficient
 C_p pressure coefficient
 F, G fluxes of mass, momentum and energy
 F_v, G_v viscous terms of the Navier-Stokes formulation
 F^+ non-dimensional actuator frequency, fc/U_∞
 H width of the orifice, m
 I identity matrix
 M free-stream Mach number
 \mathbf{M} transformation matrix from conserved variables to primitive variables $\partial Q/\partial q$
 Q conservation variables
 Pr Prandtl number
 Re Reynolds number, $\frac{\rho_\infty a_\infty c}{\mu_\infty}$
 St actuator Strouhal number, fH/V_0
 T temperature, $^\circ C$
 U, V contravariant velocities
 U_{jet} spatial mean jet velocity from actuator
 U_∞ free-stream velocity, m/s
 a speed of sound, m/s
 c chord length, m
 e total energy
 f actuator forcing frequency, Hz
 p pressure, nondimensionalized by γp_∞
 q primitive variables
 r distance outward from body
 t time, nondimensionalized by c/a_∞
 u, v Cartesian velocities in x and y direction, respectively, nondimensionalized by a_∞
 $\langle u'_{\text{jet}} \rangle$ RMS velocity of the actuator jet oscillations
 x, y Cartesian coordinates
 Δt time step (nondimensional)
 α angle of attack (degrees)
 δ difference operator
 γ ratio of specific heats
 λ coefficient of bulk viscosity
 μ viscosity
 ρ density
 τ_{ij} viscous stress tensor
 ζ, η, ξ curvilinear coordinate directions

*NRC Research Fellow, Flow Physics and Control Branch, NASA Langley Research Center, Mail Stop 170, Hampton, VA 23681

[†]Currently assistant professor, Department of Mathematics, University of Alabama, Huntsville, AL 35899 (ravindra@ultra.math.uah.edu).

Subscripts

max	maximum
min	minimum
x, y	denotes differentiation in x and y directions, respectively
η, ζ	denotes differentiation in η and ζ directions, respectively
$()_\infty$	free-stream condition

Superscripts

n	denotes time level
()	denotes quantities in generalized coordinates
+	denotes positive and negative flux conditions
-	

I. Introduction

The experimental and computational investigations of active control of flow past airfoils at high angles of attack is an area of active research as extending the usable angles of attack has many important applications. There are a number of articles showing the effectiveness of flow control for airfoils. For example, in [10] leading edge suction was investigated for transition delay, in [23] jet flaps were employed for lift increase and in [6] surface suction/blowing was used to rapidly change lift and drag on rotary wing aircraft. However, most of the control techniques considered in the past required relatively more power input or involved weight and complexity penalties.

In [1], [2] and [18], an innovative method for active control has been experimentally demonstrated using the so-called synthetic jet. The synthetic jet actuator produces a high-frequency jet from the surrounding fluid with zero net mass input. A novel feature of this actuator is that it requires only electrical power. In [1] and [18], a synthetic jet was used to produce a larger jet and in [2] a pair of actuators were used to show significant lift on cylinders. In another experimental work, Seifert et al [15] have investigated unsteady suction and blowing on a symmetric airfoil to increase post-stall lift. They show by introducing an unsteady jet near the leading edge tangential to the surface of a NACA0015 airfoil significant increase in lift can be obtained with relatively low momentum input. They also observed re-attachment of the flow

and elimination of large wake region above the attached region. Later Seifert et. al. [16] and Seifert and Pack [17], investigated the dependence of actuator location, momentum coefficient of the jet and frequency of the oscillation, and performance in higher Reynolds number.

Some of the recent numerical simulations reported in [21, 6, 5] also support these findings. In [21], a periodic blowing and suction normal to the surface was used at 2.5% chord from the leading edge of a NACA0012 airfoil. They showed that lift was increased for angles of attack between 18° – 35° . They used the Reynolds average Navier-Stokes (RANS) approach with the Baldwin-Lomax algebraic turbulence model. Hassan et. al. [6] have also used RANS approach with Baldwin-Lomax turbulence model. In their work zero net mass suction/blowing was placed at 13% chord and they found out that for certain oscillation frequency and peak amplitude, the lift can be increased albeit with high momentum input. The comparison with experiments were not given in both of these works. Finally, Donovan et. al. [5] reported numerical investigations of both steady and unsteady jet on airfoils. They used an unsteady RANS incompressible flow solver with Spalart-Allmaras [19] turbulence model and compared their results with the experiments of [15]. Performance improvements were obtained by placing the actuator near the airfoil leading edge. A significant lift increase of about 29% was obtained using synthetic jet actuators in the post-stall regime. However, their simulations assumed incompressibility which is not strictly valid as the Mach number in the experiments of Seifert [15] was $M = 0.15$.

In this article, we present a numerical investigation of unsteady suction and blowing on an airfoil using a compressible flow solver CFL3D [9]. We build upon the previous work of Donovan et al [5] to validate CFL3D for active flow control applications and to address some of the anomalies in the previous reports.

The plan of the paper is as follows. In §II, we will present the governing equations. In §III, we will present the computational methods used to solve them. In §IV, we will present numerical results for the baseline case. In §V, we will present numerical results for the active control case. In §VI, we conclude the paper with a summary.

II. The Governing Equations

The governing equations considered are the time-dependent, viscous compressible Navier-Stokes equations. The non-dimensional form of these equations in Cartesian coordinates for an ideal gas are

$$\frac{\partial \mathbf{Q}}{\partial t} + \frac{\partial \mathbf{F}}{\partial x} + \frac{\partial \mathbf{G}}{\partial y} = \frac{1}{Re} \left(\frac{\partial \mathbf{F}_v}{\partial x} + \frac{\partial \mathbf{G}_v}{\partial y} \right) \quad (1)$$

where \mathbf{Q} , \mathbf{F} and \mathbf{G} are the flux vectors given by

$$\mathbf{Q} = \begin{bmatrix} \rho \\ \rho u \\ \rho v \\ e \end{bmatrix}, \mathbf{F} = \begin{bmatrix} \rho u \\ \rho u^2 + p \\ \rho uv \\ (e + p)u \end{bmatrix}, \mathbf{G} = \begin{bmatrix} \rho v \\ \rho uv \\ \rho v^2 + p \\ (e + p)v \end{bmatrix}.$$

The viscous flux vectors, \mathbf{F}_v and \mathbf{G}_v are defined as

$$\mathbf{F}_v = \begin{bmatrix} 0 \\ \tau_{xx} \\ \tau_{xy} \\ f_4 \end{bmatrix}, \mathbf{G}_v = \begin{bmatrix} 0 \\ \tau_{xy} \\ \tau_{yy} \\ g_4 \end{bmatrix}.$$

where

$$\tau_{xx} = \frac{2}{3}\mu(2u_x - v_y) \quad \tau_{xy} = \mu(u_y - v_x),$$

$$\tau_{yy} = \frac{2}{3}\mu(2v_y - u_x),$$

$$f_4 = u\tau_{xx} + v\tau_{xy} + \frac{\mu}{Pr}(\gamma - 1)^{-1} \frac{\partial a^2}{\partial x}$$

$$g_4 = u\tau_{xy} + v\tau_{yy} + \frac{\mu}{Pr}(\gamma - 1)^{-1} \frac{\partial a^2}{\partial y}.$$

Here the Prandtl number, Pr , is

$$Pr = \frac{\mu c_p}{\kappa_\infty}$$

where c_p is the specific heat at constant pressure, and κ is the coefficient of thermal conductivity. The pressure is defined by the equation of state for an ideal gas:

$$p = (\gamma - 1)[e - \frac{\rho}{2}(u^2 + v^2)], \quad (2)$$

where $\gamma = \frac{c_p}{c_v}$, and has a value of 1.4 for air. The speed of sound, a , is defined as $a^2 = \gamma \frac{p}{\rho}$. The Reynolds number is defined as $Re = \frac{\rho_\infty a_\infty l}{\mu_\infty}$, where l refers to a chord length and the subscript, ∞ , refers to free stream quantities. The dynamic viscosity, μ , is approximated by Sutherland formula

and equation (1) is closed by Stokes hypothesis for bulk viscosity ($\lambda + 2\mu/3$).

A. The Coordinate Transformations

In order to apply the numerical algorithm and boundary conditions easily, the governing equations which are derived in the Cartesian coordinates, (x, y) , must be transformed to the computational domain or generalized coordinates, (ξ, η) . The transformation from Cartesian coordinates to general curvilinear coordinates for two-dimensions are

$$\tau = t, \quad \xi = \xi(x, y, t), \quad \eta = \eta(x, y, t).$$

These coordinates conform to the surface of the body and maps the original Cartesian space (x, y) or physical domain onto a computational domain (ξ, η) , which is rectangular with a uniform mesh. In terms of these curvilinear coordinates the Navier-Stokes equations become

$$\frac{\partial \hat{\mathbf{Q}}}{\partial \tau} + \frac{\partial \hat{\mathbf{F}}}{\partial \xi} + \frac{\partial \hat{\mathbf{G}}}{\partial \eta} = \frac{1}{Re} \left(\frac{\partial \hat{\mathbf{F}}_v}{\partial \xi} + \frac{\partial \hat{\mathbf{G}}_v}{\partial \eta} \right), \quad (3)$$

where

$$\hat{\mathbf{Q}} = J^{-1} \begin{bmatrix} \rho \\ \rho u \\ \rho v \\ e \end{bmatrix}, \quad \hat{\mathbf{F}} = J^{-1} \begin{bmatrix} \rho U \\ \rho u U + p \xi_x \\ \rho v U + p \xi_y \\ (e + p)U - \xi_t p \end{bmatrix},$$

$$\hat{\mathbf{G}} = J^{-1} \begin{bmatrix} \rho V \\ \rho u V + p \eta_x \\ \rho v V + p \eta_y \\ v(e + p) - \eta_t p \end{bmatrix}.$$

with

$$U = \xi_t + \xi_x u + \xi_y v, \quad V = \eta_t + \eta_x u + \eta_y v,$$

where U and V are the contravariant velocities. In curvilinear coordinates the viscous flux terms are given by

$$\hat{F}_v = J^{-1}(\xi_x F_v + \xi_y G_v) \text{ and } \hat{G}_v = J^{-1}(\eta_x F_v + \eta_y G_v),$$

where $J = \frac{\partial(\xi, \eta, \tau)}{\partial(x, y, t)}$. Similarly, the stress terms in F_v and G_v are also transformed.

III. Computational Algorithm

In this study the algorithm used to solve the Navier-Stokes equations is the CFL3D code reported in [9]. CFL3D solves the time-dependent conservation law form of the Reynolds-averaged Navier-Stokes equations. The spatial discretization involves a semi-discrete finite-volume approach. Upwind-biasing is used for the convective and pressure terms, while central differencing is used for the shear stress and heat transfer terms. Time advancement is implicit with the ability to solve steady or unsteady flows [13], [14], [20], [12]. Multi-grid and mesh sequencing are available for convergence acceleration.

A. Time Differencing

The Navier-Stokes equations (3) are discretized in time using the backward Euler implicit scheme and then the resulting nonlinear system is linearized in time about \hat{Q}^n to obtain

$$\left[\frac{I}{\Delta t} + \delta_\xi A^n + \delta_\eta B^n\right] \Delta \hat{Q}^n = R(\hat{Q}^n), \quad (4)$$

where

$$R = -\left[\frac{\partial}{\partial \xi} \left(\hat{F} - \frac{1}{Re} \hat{F}_v\right) + \frac{\partial}{\partial \eta} \left(\hat{G} - \frac{1}{Re} \hat{G}_v\right)\right],$$

$$\Delta \hat{Q}^n = \hat{Q}^{n+1} - \hat{Q}^n, \quad A = \frac{\partial}{\partial \hat{Q}} \left(\hat{F} - \frac{1}{Re} \hat{F}_v\right)$$

and

$$B = \frac{\partial}{\partial \hat{Q}} \left(\hat{G} - \frac{1}{Re} \hat{G}_v\right).$$

Approximate factorization

The central difference discretization to Equation (3) results in a large banded square matrix which is sparse but would be computationally expensive. To overcome this problem an approximate factorization is introduced which converts the two-dimensional operator into one-dimensional operators:

$$\left[\frac{\mathbf{M}}{\Delta t} + \frac{\partial}{\partial \xi} A^*\right] \Delta q' = R(q^n)$$

$$\left[\frac{\mathbf{M}}{\Delta t} + \frac{\partial}{\partial \eta} B^*\right] \Delta q^n = \frac{M}{\Delta t} \Delta q'$$

and

$$q^{n+1} = q^n + \Delta q^n, \quad (5)$$

where $q = (\rho, u, v, p)$,

$$\mathbf{M} = \frac{\partial Q}{\partial q}, \quad A^* = \frac{\partial}{\partial q} \left(\hat{F} - \frac{1}{Re} \hat{F}_v\right),$$

and

$$B^* = \frac{\partial}{\partial q} \left(\hat{G} - \frac{1}{Re} \hat{G}_v\right).$$

This factorization yields two block tridiagonal inversions for each sweep. Prior to the execution of Equation (5), the corrections are constrained in order to maintain the positivity of the thermodynamic scalars ρ and p . For example, the update to pressure is taken as

$$p^{n+1} = p^n + \Delta \left[1 + \phi_c \left(\alpha_c + \left|\frac{\Delta p}{p^n}\right|\right)\right]^{-1}$$

whenever $\frac{\Delta p}{p^n} \leq \alpha_c$, where $\alpha = -0.2$ and $\phi_c = 2.0$.

B. Spatial Differencing

The spatial differencing is done using a second-order-accurate upwind-biased scheme. The fluxes \hat{F} , \hat{G} representing pressure and convective terms are differenced using up-winding and a flux-vector-splitting method. For example, the flux difference in the ξ direction is

$$\partial_\xi \hat{F} = \partial_\xi^- \hat{F}^+ + \partial_\xi^+ \hat{F}^-.$$

The flux vector splitting is due to Van Leer. The flux \hat{F} , for example, is split according to the contravariant Mach number in the ξ direction, see [9]. The split-flux differences are implemented as a flux balance across the i th cell holding spatial indices j and k constant as

$$\begin{aligned} & \partial_\xi^- \hat{F}_i^+ + \partial_\xi^+ \hat{F}_i^- \\ &= [\hat{F}^+(Q^-) + \hat{F}^-(Q^+)]_{i+1/2} \\ & - [\hat{F}^+(Q^-) + \hat{F}^-(Q^+)]_{i-1/2}, \end{aligned}$$

where $\hat{F}^+(Q^-)_{i+1/2}$ denotes a forward flux evaluated using the metric terms at the cell interface $(i + 1/2)$, and state variables are obtained by fully upwind second-order interpolation of cell-centered variables

$$Q_{i+1/2}^- = (3/2)Q_i - (1/2)Q_{i-1},$$

$$Q_{i+1/2}^+ = (3/2)Q_{i+1} - (1/2)Q_{i+2}.$$

The diffusion terms are differenced using a second order central differencing:

$$(\partial_{\xi} \widehat{F}_v)_i = (\widehat{F}_v)_{i+\frac{1}{2}} - (\widehat{F}_v)_{i-\frac{1}{2}}.$$

C. Convergence Acceleration

A sequence of grids $G_0, G_1, G_2, \dots, G_N$ is defined, where G_N denotes the finest grid and coarser grids are formed by successively deleting every other line in all coordinate directions. The fine grid serves to damp the high-frequency errors while the coarser grids damp the low-frequency errors. The coarse grids are solved with a forcing function on the right-hand side, arising from restricting the residual from the finer grids. The forcing function is the relative truncation error between the grids, such that the solution on the coarser meshes are driven by the fine grid residual. A fixed cycling strategy (W-cycle) is used for the results presented. The solution were smoothed on each grid through five steps before switching to the next mesh.

D. Turbulence Models

In order to predict turbulent flows by solving the Reynolds averaged Navier-Stokes equations, closure assumptions must be made about the turbulent stress and heat-flux quantities. For separated unsteady flow computations using Reynolds averaged Navier-Stokes equations, choosing the appropriate turbulence models is not trivial. Among the available models, the Spalart-Allmaras (SA) model has been shown to be effective for a variety of flows including 2-D separated airfoil flows, see [5] and [8]. The Spalart-Allmaras model is a one equation model which solves a single transport equations for a modified turbulent viscosity.

VI. Baseline Simulations

The airfoil configuration used here is the one used at Tel-Aviv University (TAU) for low-speed wind tunnel test. This airfoil, we call it TAU0015, has a 0.4% chord notch at the leading edge and a 3% chord thick trailing edge, otherwise is a NACA0015 airfoil. In order to lay a single-block structured grid around the airfoil, the original airfoil was modified to smooth out the square corners at the leading

edge actuator. Figure 1 shows this modification in comparison with the original TAU0015 airfoil with the leading edge actuator. The baseline simulations given in this section uses no actuation. The following parameters were used in the simulations which are the same as in the experimental conditions: the Mach number of 0.15 and a chord Reynolds number of 1.2×10^6 . The computations were performed using a 417X129 C-grid shown in Figure 2 with a minimum normal spacing of 0.0000015c.

The boundary conditions applied are no-slip with no normal velocity at the body surface. Along the far-field upstream and the circumferential boundaries, a quasi-one-dimensional characteristic analysis is used to determine the boundary data, assuming free-stream conditions exterior to the boundary. Along the downstream boundary, first-order extrapolation of the conserved variables is used. The outer boundary is sufficiently far away, $r_{\max} = 12c$, from the airfoil, thereby minimizing the effects of the outer boundary on the flow over the airfoil.

Figure 3 shows the enlarged view around leading-edge showing the grid near the actuator. Figure 4 shows the computed lift coefficients versus angle of attack computed with experimental data. The results show very good agreement before stall, but deviate from the experimental data at stall, similar to the results of [5]. A drag polar is shown in Figure 4 for the baseline case which also shows good agreement with experiment at lower angles of attack but deviate from the experimental values for post-stall angles of attack. Similar observations were made in [5] and [7] using the same airfoil and turbulence model but with different numerical methods and models.

In [7] an unstructured grid was employed to study the effects of smoothing the square corners at the leading-edge actuator. Both the original TAU0015 and the modified TAU0015; see Figure 1, were studied for the baseline case. They found remarkable agreement between modified and original TAU0015 airfoil computations but original TAU0015 model stalled before the modified TAU0015 model resulting in some disagreement in the post-stall region. They concluded that the discrepancies between computed and experimental results was due to the way aerodynamic properties were computed and thus a proper interpretation of the experimental results is important. For example, experimental measurements used discrete

pressure taps and hence the lift coefficient consists of the pressure contribution only and leading edge actuator region was not included in the computation. This was verified in [7] by recomputing the lift without including the actuator portion at the leading edge.

We note here that we did not go back and recompute lift and drag; rather because the comparisons in Figures 4–5 are sufficiently good that the remainder of the paper will focus on this conditions.

V. Control Simulations

In this section, we present some numerical simulations of synthetic jet control and compare them with experiments. The experiments that we selected here for comparison used a leading-edge unsteady jet tangential to the surface.

A. Actuator Boundary Conditions

In all the calculations the synthetic jet actuator is modified using suction and blowing type boundary condition by prescribing velocity at the surface. The velocity boundary condition is given by

$$\mathbf{u}(x, 0, t) = A \sin(\omega t) f(\mathbf{x}),$$

where the amplitude $A = \sqrt{\frac{c}{2H}} U_\infty \sqrt{2 \langle C_\mu \rangle}$, the prescribed frequency of oscillation $\omega = (F^+ U_\infty / 2\pi c)$, the spatial distribution $f(\mathbf{x}) = 1$, F^+ is the non-dimensional frequency and the oscillatory momentum blowing coefficient $\langle C_\mu \rangle$ is defined as

$$\langle C_\mu \rangle = 2(H/c) \langle u_{\text{jet}} \rangle / U_\infty^2.$$

The same C-grid used in the baseline simulations was used here. The jet at the slot was resolved using a fine grid consisting of twenty grid points.

B. Numerical Results

The parameters Mach number and Reynolds number were taken to be the same as in the baseline case. The experiments included various blowing coefficients $\langle C_\mu \rangle$, with $F^+ = 0.58$. To assess the effectiveness of synthetic jets, various blowing coefficients were tested at fixed post-stall

angle-of-attacks $\alpha = 22^\circ$, $\alpha = 24^\circ$ and a range of $\langle C_\mu \rangle$ were used in the simulations. The turbulence model used was again Spalart-Allmaras with the time step $\Delta t = 0.00005$. In order to reduce the computational time required to converge to a solution with blowing, the baseline case solution was used as the initial flow conditions for the blowing computations.

The variation of ΔC_l with blowing coefficients $\langle C_\mu \rangle$ for $\alpha = 22^\circ$ is shown in Figure 6. The incremental lift increases as the momentum blowing coefficient increase for both the experimental and computational data in much better agreement than reported in [5]. The computational results over/under-predict lift. This may be due to inability of the turbulence model's to predict separated flows, inconsistency in the actuator geometry or the lack of grid resolution. Figure 7 shows the analogous variation in ΔC_l with blowing coefficients $\langle C_\mu \rangle$ for $\alpha = 24^\circ$. The computed ΔC_l increase smoothly with increasing $\langle C_\mu \rangle$ unlike the $\alpha = 22^\circ$ case. For the uncontrolled flow, a large region of separated flow was seen with two coherent structures on the suction surface. The application of control makes the flow more attached which is consistent with the works of [4] and [5].

Figure 8 shows surface pressure distribution for the baseline and controlled cases. Figure 9 and Figure 10 show the lift coefficient time histories with synthetic jet control as a function of non-dimensional time ($\frac{t a_\infty}{c}$) for $\alpha = 22^\circ$ and $\alpha = 24^\circ$, respectively. Note that approximately 40 non-dimensional times were necessary to obtain a statistically stationary solution.

VII. Summary

A computational investigation of tangential unsteady suction and blowing for separation control on an airfoil has been performed. The effects of zero net mass suction and blowing on lift increase were studied. The computed results were compared with available wind tunnel test results to determine the accuracy of the computational results. The numerical solutions were obtained by solving the Reynolds averaged Navier-Stokes equations. A grid resolution study was conducted using baseline (uncontrolled) case to determine the appropriate grid density. The computed baseline results agreed reasonably with experimental results. For the active

control case, various blowing coefficients were investigated at two angles of attack, $\alpha = 22^\circ$ and $\alpha = 24^\circ$. The computed results were compared with the experiments from TAU. The results show reasonable agreement with the trends observed in the experiment.

In general, the computations showed that the lift increased as the blowing coefficient increased. In all the control simulations, the grid resolution in general and time step-size in particular was found to be critical.

Computational simulations shows that tangential unsteady suction and blowing on airfoil can be used as a means of separation control to generate lift.

Acknowledgments

The author would like to thank Dr. Avi Seifert for providing the experimental data and for many useful technical discussions. This work was supported in part by the National Aeronautics and Space Administration under NASA Contract NASW-8154 while the author was an NRC resident research associate under the supervision of Dr. Ronald Joslin. The CRAY time was provided by the Numerical Aerodynamic Simulation facility at NASA Ames Research Center.

References

- [1] M.G. ALLEN AND A. GLEZER, *Jet Vectoring Using Zero Mass Flux Control Jets*, AFOSR Contractor and Grantee Meeting on Turbulence and Internal Flows, Wright Patterson AFB, May 1995.
- [2] M. AMITAY, A. HONOHAN, M. TRAUTMAN AND A. GLEZER, *Modification of Lifting Body Aerodynamics Using Synthetic Jet Actuators*, AIAA Paper 98-0209.
- [3] R.C. CHANG, F.B. HSIAO AND R.N. SHYU, *Forcing Level Effects of Internal Acoustic Excitation on the Improvement of Airfoil Performance*, *Journal of Aircraft*, **29**(5) 1992.
- [4] A. DARABI AND I. WYGNANSKI, *On the Mechanism Responsible for Forced Flow Reattachment* Proceedings of the EUROMECH Colloquium: Active Control of Turbulent Shear Flows, Tech. Uni. Berlin, March 1997.
- [5] J.F. DONOVAN, LINDA D. KRAL AND A.W. CARY, *Active Control Applied to an Airfoil*, AIAA Paper 98-0210, 1998.
- [6] A.A. HASSAN AND R.D. JANAKIRAM, *Effects of Zero-mass Synthetic jets on the Aerodynamics of the NACA-0012 Airfoil*, AIAA 97-2326, 1997.
- [7] R.D. JOSLIN, L.G. HORTA AND F.J. CHEN, *Transitioning Active Flow Control to Applications*, AIAA Paper 99-3575, 1999.
- [8] S. KO AND W.J. MCCROSKEY, *Computations of Unsteady Separating Flows Over an Oscillating Airfoil*, AIAA Paper 95-0312, 1997.
- [9] S.L. KRIST, R.T. BIEDRON AND C.L. RUMSEY, *CFL3D User's Manual*, NASA TM 1998-208444.
- [10] D. V. MADDALON, F. S. COLLIER, F. S. MONTOYA AND C. K. LAND, *Transition Flight Experiments on a Swept Wing with Suction*, AIAA Paper 89-1893.
- [11] V. J. MODI, F. MOKHTARIAN, M. FERNANDO AND T. YOKOMIZO, *Moving Surface Boundary-Layer Control as Applied to Two-Dimensional Airfoils*, *J. Aircraft*, Vol. 28, 1991, pp. 104-112.
- [12] G. OSWALD, K. GHIA AND U. GHIA, *An Implicit Time Marching Method for Studying Unsteady Flow with Massive Separation*, AIAA Paper 85-1489, 1985
- [13] C. RUMSEY, *Time-Dependent Navier-Stokes Computations of Separated Flows Over Airfoils*, AIAA Paper 85-1684, 1985.
- [14] C. RUMSEY, J.L. THOMAS, G.P. WARREN AND G.C. LIU, *Upwind Navier-Stokes Solutions for Periodic Flows*, AIAA Paper 86-0247, 1986.
- [15] A. SEIFERT, T. BACHAR, D. KOSS, M. SHEPSHELOVICH AND I. WYGNANSKI, *Oscil-*

latory Blowing: A Tool to Delay Boundary-Layer Separation, AIAA Journal, **31**(11) 1993.

- [16] A. SEIFERT, A. DARABI AND I. WYGANSKI, *Delay of Airfoil Stall by Periodic Excitation*, Journal of Aircraft, **33**(4) 1996.
- [17] A. SEIFERT AND L. G. PACK, *Oscillatory Control of Separation at High Reynolds Numbers*, AIAA Paper 98-0214.
- [18] B. L. SMITH AND A. GLEZER, *Vectoring and Small Scale Motions Effected in Free Shear Flows Using Synthetic Jet Actuators*, AIAA Paper 97-0213.
- [19] P.R. SPALART AND S.R. ALLMARAS, *A One Equation Turbulence Model for Aerodynamic Flows*, AIAA Paper 92-0439, 1992.
- [20] J. THOMAS AND R. WALTERS, *Upwind Relaxation Algorithms for the Navier-Stokes Equations*, AIAA Paper 85-1501, 1985.
- [21] J.M. WU, X.Y. LU, A.G. DENNEY AND M. FAN, *Post-Stall Lift Enhancement on an Airfoil by Local Unsteady Control, Part I. Lift, Drag and Pressure Characteristics*, AIAA 97-2063.
- [22] J.M. WU, X.Y. LU AND J.Z. WU, *Post-Stall Lift Enhancement on an Airfoil by Local Unsteady Control, Part II. Mode Competition and Vortex Dynamics*, AIAA 97-2064.
- [23] H. YOSHIHARA AND D. ZONARS, *The Transonic Jet Flap- A Review of Recent Results*, Proceedings. SAE National Aerospace & Manufacturing Meeting, November 1975.

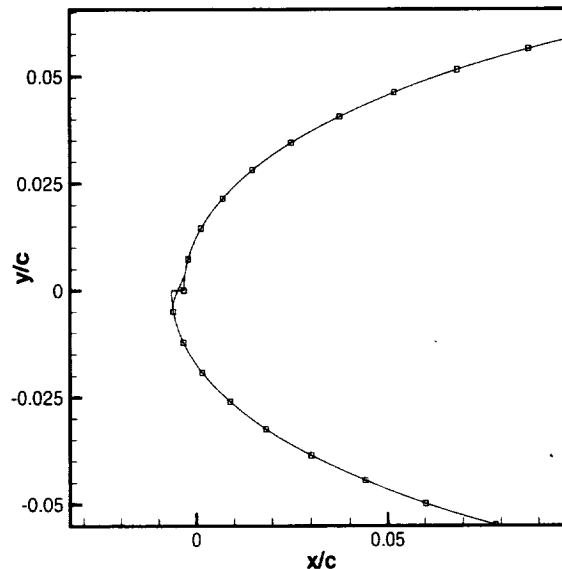


FIG. 1 Leading edge regions of TAU0015 and modified TAU0015 airfoils.

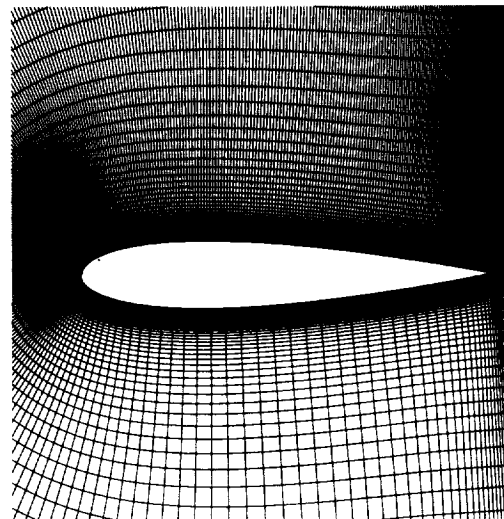


FIG. 2 TAU0015 airfoil 417×129 C-grid, $\Delta r_{\min} = 0.0000015c$, $r_{\max} = 12c$.

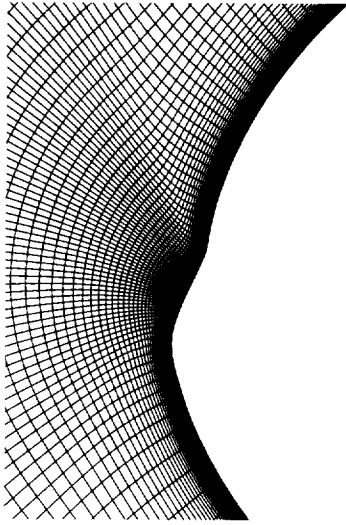


FIG. 3 Blowup of the TAU0015 airfoil near the leading edge.

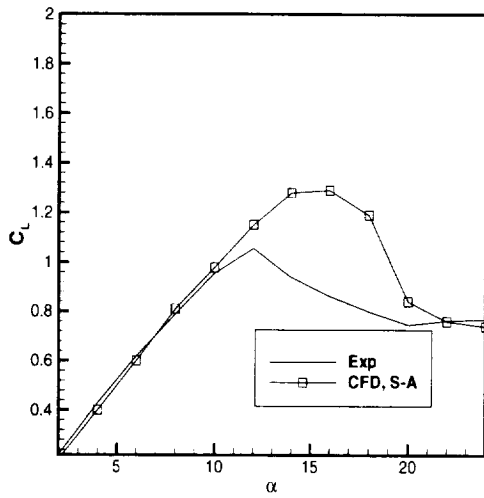


FIG. 4 Baseline lift coefficient for TAU0015 airfoil computed with experiments.

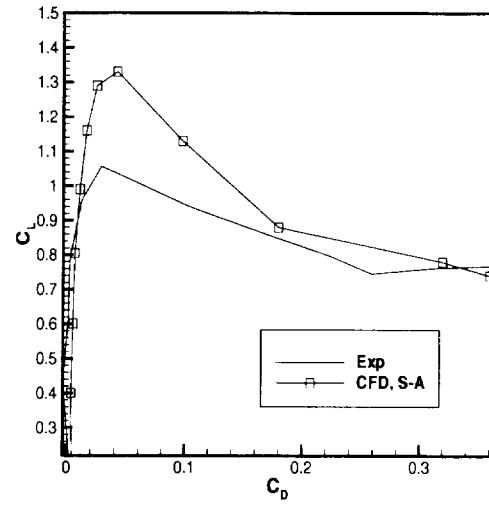


FIG. 5 Baseline drag polar for TAU0015 airfoil compared with experiments.

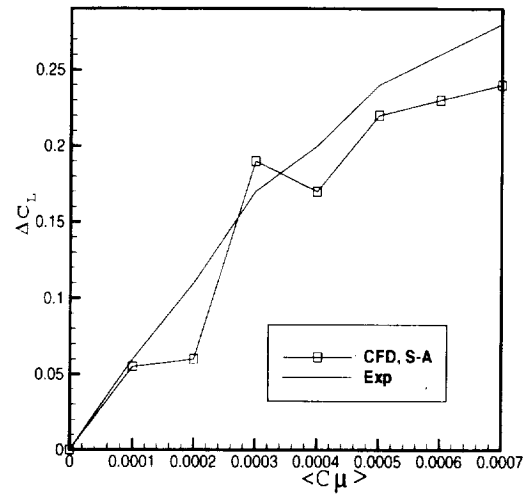


FIG. 6 ΔC_L versus $\langle C_\mu \rangle$ for the TAU0015 airfoil at $\alpha = 22^\circ$ compared with experiments.

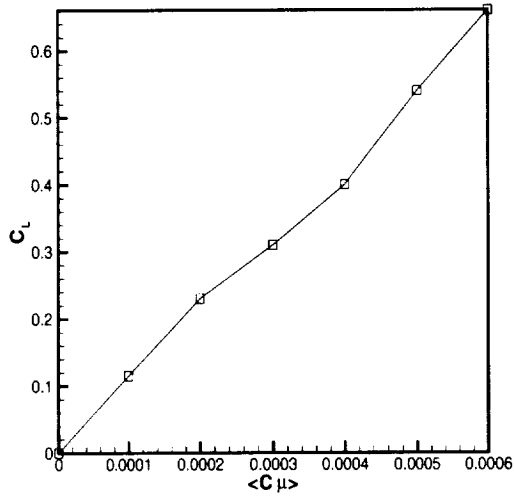


FIG. 7 ΔC_L versus $\langle C_\mu \rangle$ for the TAU0015 airfoil at $\alpha = 24^\circ$.

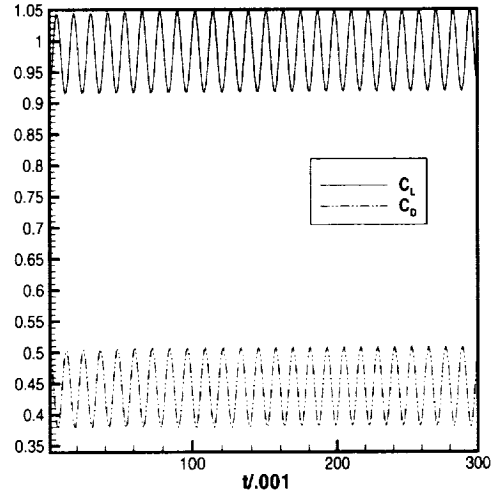


FIG. 9 Lift and Drag history of time accurate calculations of TAU0015 airfoil for $M=0.15$, $Re = 1.2 \times 10^6$, $\alpha = 22^\circ$, $f^+ = 0.58$ and $\langle C_\mu \rangle = 0.0003$.

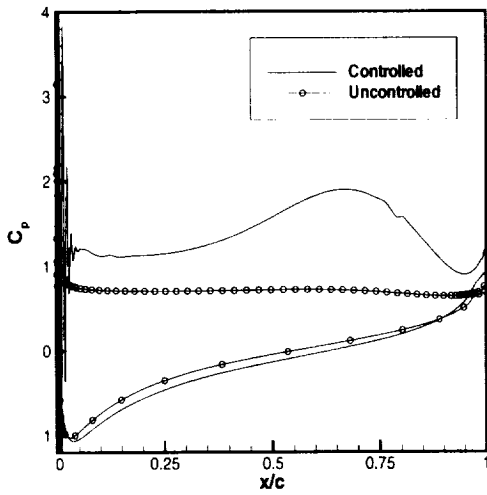


FIG. 8 Pressure distribution on TAU0015 airfoil at $Re = 1.2 \times 10^6$, $M=0.15$, $\alpha = 24^\circ$, $F^+ = 0.58$ and $\langle C_\mu \rangle = 0.0006$.

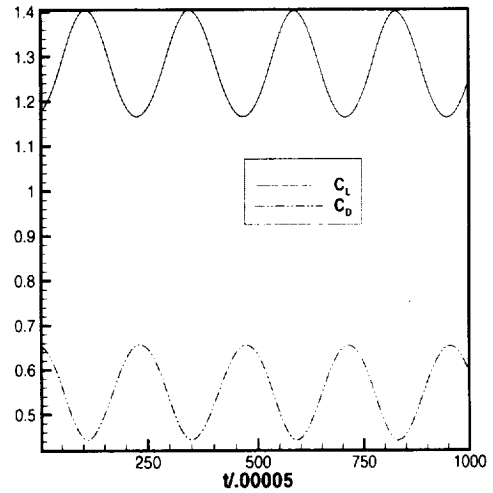


FIG. 10 Lift and Drag history of time accurate calculations of TAU0015 airfoil for $M=0.15$, $Re = 1.2 \times 10^6$, $\alpha = 24^\circ$, $f^+ = 0.58$ and $\langle C_\mu \rangle = 0.0005$.

REPORT DOCUMENTATION PAGE			Form Approved OMB No. 0704-0188	
Public reporting burden for this collection of information is estimated to average 1 hour per response, including the time for reviewing instructions, searching existing data sources, gathering and maintaining the data needed, and completing and reviewing the collection of information. Send comments regarding this burden estimate or any other aspect of this collection of information, including suggestions for reducing this burden, to Washington Headquarters Services, Directorate for Information Operations and Reports, 1215 Jefferson Davis Highway, Suite 1204, Arlington, VA 22202-4302, and to the Office of Management and Budget, Paperwork Reduction Project (0704-0188), Washington, DC 20503				
1. AGENCY USE ONLY (Leave blank)		2. REPORT DATE December 1999	3. REPORT TYPE AND DATES COVERED Technical Memorandum	
4. TITLE AND SUBTITLE Active Control of Flow Separation Over an Airfoil			5. FUNDING NUMBERS WU 706-32-21-02	
6. AUTHOR(S) S. S. Ravindran				
7. PERFORMING ORGANIZATION NAME(S) AND ADDRESS(ES) NASA Langley Research Center Hampton, VA 23681-2199			8. PERFORMING ORGANIZATION REPORT NUMBER L-17932	
9. SPONSORING/MONITORING AGENCY NAME(S) AND ADDRESS(ES) National Aeronautics and Space Administration Washington, DC 20546-0001			10. SPONSORING/MONITORING AGENCY REPORT NUMBER NASA/TM-1999-209838	
11. SUPPLEMENTARY NOTES Ravindran: NRC-Resident Research Associate, Langley Research Center, Hampton, VA				
12a. DISTRIBUTION/AVAILABILITY STATEMENT Unclassified-Unlimited Subject Category 02 Distribution: Nonstandard Availability: NASA CASI (301) 621-0390			12b. DISTRIBUTION CODE	
13. ABSTRACT (Maximum 200 words) Designing an aircraft without conventional control surfaces is of interest to aerospace community. In this direction, smart actuator devices such as synthetic jets have been proposed to provide aircraft maneuverability instead of control surfaces. In this article, a numerical study is performed to investigate the effects of unsteady suction and blowing on airfoils. The unsteady suction and blowing is introduced at the leading edge of the airfoil in the form of tangential jet. Numerical solutions are obtained using Reynolds-Averaged viscous compressible Navier-Stokes equations. Unsteady suction and blowing is investigated as a means of separation control to obtain lift on airfoils. The effect of blowing coefficients on lift and drag is investigated. The numerical simulations are compared with experiments from the Tel-Aviv University (TAU). These results indicate that unsteady suction and blowing can be used as a means of separation control to generate lift on airfoils.				
14. SUBJECT TERMS Active Flow Control; separation control; time-accurate CFD; Oscillatory control; synthetic jets			15. NUMBER OF PAGES 15	
			16. PRICE CODE A03	
17. SECURITY CLASSIFICATION OF REPORT Unclassified	18. SECURITY CLASSIFICATION OF THIS PAGE Unclassified	19. SECURITY CLASSIFICATION OF ABSTRACT Unclassified	20. LIMITATION OF ABSTRACT UL	